

Structural and complex impedance spectroscopic studies of $\text{Ni}_{0.5}\text{Mg}_{0.3}\text{Cu}_{0.2}\text{Fe}_2\text{O}_4$ ferrite nanoparticle

Mohamed Houcine Dhaou^{1,2} · Sobhi Hcini^{3,4} · Abdulrahman Mallah⁵ · Mohamed Lamjed Bouazizi⁶ · Abdelmajid Jemni¹

Received: 17 September 2016 / Accepted: 4 December 2016 / Published online: 16 December 2016
© Springer-Verlag Berlin Heidelberg 2016

Abstract Spinel ferrite having composition $\text{Ni}_{0.5}\text{Mg}_{0.3}\text{Cu}_{0.2}\text{Fe}_2\text{O}_4$ was prepared by the sol-gel technique at 1473 K. The X-ray diffraction results indicate that the ferrite sample has a cubic spinel-type structure with $Fd\bar{3}m$ space group. The electrical properties of the studied sample using complex impedance spectroscopy technique have been investigated in the frequency range 10^2 – 10^7 Hz and in the temperature range 300–500 K. The total conductivity curves for sample are found to obey Jonscher power law ($\sigma(\omega) = \sigma_{\text{dc}} + A\omega^n$) with an increase in the frequency exponent (n) as temperature increases. The activation energy deduced from the analysis of the conductivity curves matches very well with the value estimated from the relaxation time, indicating that relaxation process and electrical conductivity are attributed to the same defect.

Nyquist plots of impedance show semicircle arcs for sample, and an electrical equivalent circuit has been proposed to explain the impedance results. The effect of frequency and temperature on dielectric constant (ϵ'') and dielectric loss ($\tan\delta$) has also been discussed in terms of hopping of charge carriers between Fe^{2+} and Fe^{3+} ions.

1 Introduction

Spinel ferrite materials with general formula of MFe_2O_4 where M is a divalent cation (Mn^{2+} , Fe^{2+} , Co^{2+} , Ni^{2+} , Cu^{2+} , Zn^{2+} , etc.) have become an important class of magnetic materials due to their rich electrical and magnetic properties which depend on several factors such as method of preparation, the difference in ionic radii, microstructure changes, and chemical compositions [1, 2]. Ferrite materials have attracted the attention of the scientific community for past few decades not only for the variety of their physical properties, but also for their potential applications such as microwave devices, computer memories, transformers, magnetic recordings and storage, multilayered chip inductors, magnetocaloric refrigeration, and other devices [1, 3–6].

A way to study the electrical properties of ferrites can be achieved by the complex impedance spectroscopy (CIS) technique. This technique offers several advantages such as the determination of relaxation frequency and separation of grain, grain boundary, and grain-electrode effects. The complex impedance spectroscopic studies involve measurement of real and imaginary parts of impedance for a wide range of temperature and frequency. In recent years, this technique has become a well-accepted fundamental tool for characterizing ionic conductors in terms of ionic conductivity, electrode polarization, and activation energy

✉ Sobhi Hcini
hcini_sobhi@yahoo.fr; dhaou_2000tn@yahoo.fr

¹ Laboratory of Studies of Thermal Systems and Energy, Ibn Eljazzar Road, National Engineering School of Monastir, University of Monastir, 5019 Monastir, Tunisia
² Department of Physics, College of Science, Qassim University, Buraydah Almolaydah, Buraydah, Saudi Arabia
³ Research Unit of Valorization and Optimization of Exploitation of Resources, Faculty of Science and Technology of Sidi Bouzid, University Campus Agricultural City, University of Kairouan, 9100 Sidi Bouzid, Tunisia
⁴ Department of Physics, Faculty of Sciences of Gafsa, University Campus - Sidi Ahmed Zarroug, University of Gafsa, 2112 Gafsa, Tunisia
⁵ Department of Chemistry, College of Science, Qassim University, Buraydah Almolaydah, P.O.Box: 6644, Buraydah 51452, Saudi Arabia
⁶ College of Engineering-Prince Sattam Bin Abdulaziz University, 655, Al Kharj 11942, Saudi Arabia

for ion migration. Along this line, several studies have been reported in the literature in order to understand the electrical and dielectric properties of ferrite materials [1, 2, 7–12].

Among spinel ferrites, Ni–Mg ferrites are among the most widely used soft magnetic materials because of their use in high-frequency applications as they possess high electrical resistivity and low losses [13]. The various compositions of $\text{Ni}_{1-x}\text{Mg}_x\text{Fe}_2\text{O}_4$ system have been widely investigated and reported in the literature [14–18]. Therefore, several substitutions were made on Ni–Mg ferrite system in order to improve its practical applications. For example, Hashim et al. [19] have studied the structural, electrical, and magnetic properties of Cr-doped Ni–Mg ferrite nanoparticle. For their part, Hossain et al. [20] have investigated the magnetic properties of Mn^{2+} -substituted nanocrystalline $\text{Ni}_{0.5-x}\text{Mn}_x\text{Mg}_{0.5}\text{Fe}_2\text{O}_4$ ferrites synthesized by a combustion technique. On the other hand, *EI Hiti* studied the effect of Zn substituted on the dielectric behavior and *ac* electrical conductivity of Ni–Mg ferrites [21]. However, the reports on electrical properties using CIS technique of Ni–Mg–Cu ferrite system with the specific composition $\text{Ni}_{0.5}\text{Mg}_{0.3}\text{Cu}_{0.2}\text{Fe}_2\text{O}_4$ are not available in the literature. In this work, we choose to prepare this sample by sol–gel technique. Firstly, we presented the detailed synthesis process of our sample and then we studied its structural properties. We have also carried out complex impedance formalism and relaxation process of this sample in 300–500 K temperature range with varying frequency between 10^2 and 10^7 Hz.

2 Experimental

2.1 Synthesis process

$\text{Ni}_{0.5}\text{Mg}_{0.3}\text{Cu}_{0.2}\text{Fe}_2\text{O}_4$ sample was prepared via the sol–gel method using stoichiometric amounts of $\text{Ni}(\text{NO}_3)_2 \cdot 6\text{H}_2\text{O}$, $\text{Mg}(\text{NO}_3)_2 \cdot 6\text{H}_2\text{O}$, $\text{Cu}(\text{NO}_3)_2 \cdot 3\text{H}_2\text{O}$, and $\text{Fe}(\text{NO}_3)_3 \cdot 9\text{H}_2\text{O}$ precursors. Stoichiometric amounts of metal nitrates were first dissolved in distilled water to obtain a mixed solution. Subsequently, when these nitrates were completely dissolved in the solution, controlled amounts of citric acid were incorporated and dissolved with stirring. The molar ratio was fixed as 1:1 of nitrates to citric acid. A small amount of ammonia was added to the solution to adjust the pH value at about seven. The solution was heated on hot plate under regular stirring to 373 K followed by the addition of ethylene glycol which was used as a polymerization agent. Heating and stirring continued until obtaining a gel after about 4 h. The gel obtained was dried at 573 K to obtain a foamy dry which was ground in a mortar,

followed by drying at 773 K for 12 h in air. A powder was then obtained after a subsequent heat treatment. The powder obtained was pressed into pellets with diameter of 10 mm and thickness of about 2 mm and then sintered at 973 K for 24 h. After grinding, the pellets were pressed again and then heated at 1173 K for 24 h. In order to obtain the desired crystalline phase, the obtained pellets undergo a third cycle of grinding and repelleting and finally sintered at 1473 K during a sufficiently long annealing period (48 h). Then, all the results found in the present investigation are presented for $\text{Ni}_{0.5}\text{Mg}_{0.3}\text{Cu}_{0.2}\text{Fe}_2\text{O}_4$ ferrite nanoparticle sintered at 1473 K. The detailed synthesis process of our sample is represented in Fig. 1.

2.2 Characterization

Powder X-ray diffraction (XRD) data were collected in the 2θ range 15° – 80° with a step size of 0.0167° and a counting time of 18 s per step using a “PANalytical X’Pert Pro” diffractometer with filtered (Ni filter) Cu radiation. Standard *Si* powder was used to obtain the instrumental resolution function. Morphology of the sample was analyzed using scanning electron microscopy (SEM; Philips XL30 microscope) under an accelerating voltage of 20 kV. For electrical measurements, pure silver is deposited on the surface of pellet to ensure ohmic contact. The frequency- and temperature-dependent electrical measurements were taken using a N4L-NumetriQ (model PSM1735) connected to a computer.

3 Results and discussion

3.1 Microstructural analysis

Figure 2 presents the X-ray diffraction patterns for $\text{Ni}_{0.5}\text{Mg}_{0.3}\text{Cu}_{0.2}\text{Fe}_2\text{O}_4$ ferrite nanoparticle sintered at 1473 K. There are almost no diffraction peaks corresponding to impurity phases, suggesting that pure phase was obtained. Using “X’Pert HighScore Plus” software, the diffraction peaks are indexed with respect to the cubic spinel-type structure with the space group $Fd\bar{3}m$. The presence of diffraction planes (111), (220), (311), (222), (400), (422), (511), (440), (620), (533), (622), and (444) in the diffraction pattern confirms the formation of a cubic spinel ferrite structure. The lattice constant was calculated from the XRD data using the following equation [22, 23]:

$$a = \frac{\lambda \sqrt{h^2 + l^2 + k^2}}{2 \sin \theta} \quad (1)$$

here λ is the wavelength, a is the lattice constant, and (h k l) are the corresponding Miller indices. The obtained lattice constant is $a = 8.4185 \text{ \AA}$ that gives a cell volume of

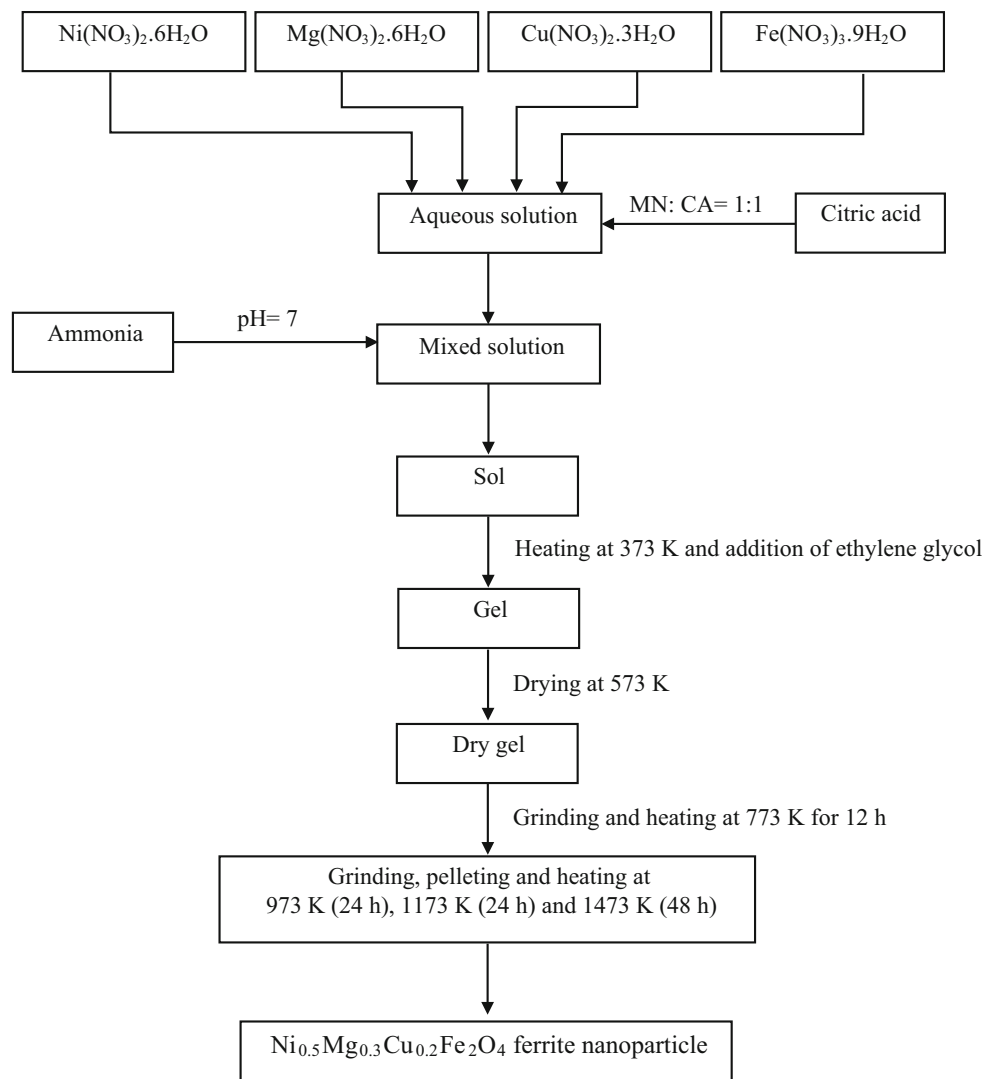


Fig. 1 Schematic diagram representing the preparation of $\text{Ni}_{0.5}\text{Mg}_{0.3}\text{Cu}_{0.2}\text{Fe}_2\text{O}_4$ ferrite nanoparticle

$V = 596.63 \text{ \AA}^3$. The X-ray density for our sample was calculated according to the following equation [22]:

$$\rho_x = \frac{8M}{Na^3} \quad (2)$$

where 8 represents the number of molecules in a unit cell of spinel lattice, M is the molecular weight of the sample, a is the lattice constant of the ferrite, and N is the Avogadro's number. The X-ray density of the sample is equal to 5.01 g/cm^3 . The obtained values of lattice constant (a) and X-ray density (ρ_x) for $\text{Ni}_{0.5}\text{Mg}_{0.3}\text{Cu}_{0.2}\text{Fe}_2\text{O}_4$ ferrite sample are higher than those obtained for the parent $\text{Ni}_{0.5}\text{Mg}_{0.5}\text{Fe}_2\text{O}_4$ ferrite nanoparticle in Refs. [14, 15]. On the one hand, the increase in lattice constant may be attributed to the higher ionic radius of Cu^{2+} (0.73 \AA) compared with that of Mg^{2+} (0.72 \AA) [24]. On the other hand, the high-density value of X-ray density can be due to the higher density of copper (8.96 g/cm^3) compared with that of magnesium (1.74 g/

cm^3). The inset of Fig. 2 shows the SEM micrograph for $\text{Ni}_{0.5}\text{Mg}_{0.3}\text{Cu}_{0.2}\text{Fe}_2\text{O}_4$ ferrite nanoparticle. The image shows unique chemical contrast corresponding to the ferrite phase, uniform grain size distribution with negligible porosity, and average particle size of about $0.56 \mu\text{m}$.

3.2 Electrical conductivity study

Frequency variation of the conductivity at different temperatures of $\text{Ni}_{0.5}\text{Mg}_{0.3}\text{Cu}_{0.2}\text{Fe}_2\text{O}_4$ ferrite nanoparticle sintered at 1473 K is shown in Fig. 3. From this figure, it can be seen that the conductivity has two types of behaviors at two regions that is valid for all temperatures. The flat region with only electronic contribution at low frequencies represents the dc conductivity. Frequency-independent conductivity can be attributed to the long-range transport of charge carriers as a response to the applied external electric field. This is totally related to the

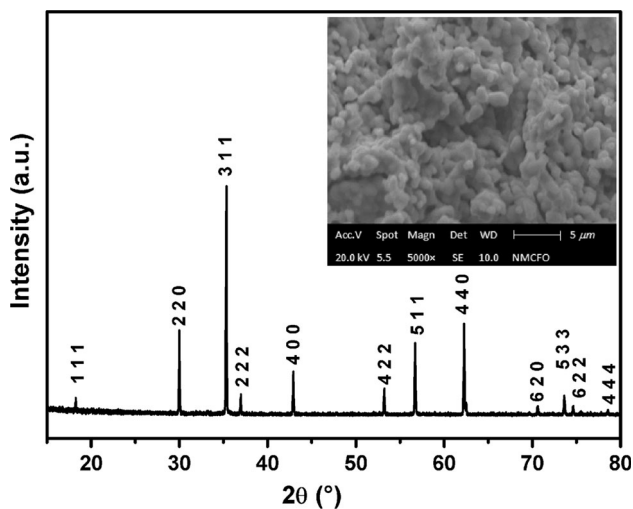


Fig. 2 XRD pattern of $\text{Ni}_{0.5}\text{Mg}_{0.3}\text{Cu}_{0.2}\text{Fe}_2\text{O}_4$ ferrite nanoparticle sintered at 1473 K. All peaks are indexed in the cubic spinel-type structure with $Fd\bar{3}m$ space group. The inset shows the SEM image

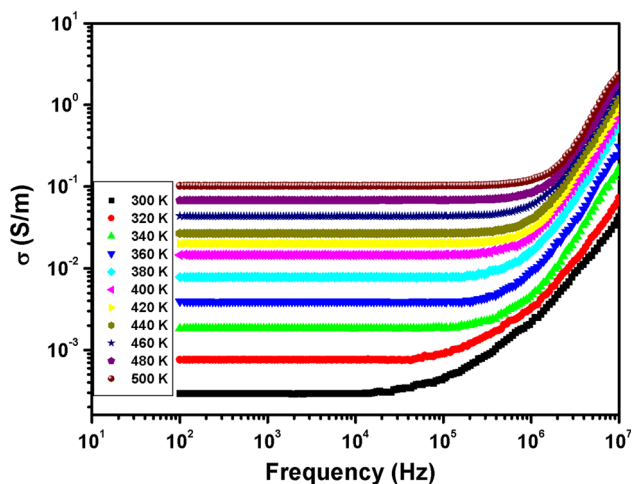


Fig. 3 Variation of the total conductivity as a function of frequency at different temperatures for $\text{Ni}_{0.5}\text{Mg}_{0.3}\text{Cu}_{0.2}\text{Fe}_2\text{O}_4$ ferrite nanoparticle sintered at 1473 K

insufficient magnitude of applied field at low frequencies to initiate hopping conductivity. Second region of conductivity which increases with frequency represents *ac* conductivity. As temperature rises, probability of electron hopping between Fe^{2+} and Fe^{3+} increases, resulting in an advancement of conductivity [25]. Therefore, *ac* conductivity increases with temperature as shown in the figure. Characteristic transition frequency between these two sites is around 10^5 Hz at 300 K and reaches to 10^6 Hz at 500 K. As seen from the figure, this frequency parameter shifts to higher values as temperature rises up. This behavior is due to the increment in the temperature of the sample by heat and a higher energy need of the mechanism which causes *ac* conductivity corresponding to higher frequencies. In

such a case, total conductivity is expressed as the sum of conductivities in these two sites. Therefore, the frequency-dependent conductivity for the sample was analyzed using universal Jonscher's power law [26]:

$$\sigma(\omega) = \sigma_{\text{dc}} + \sigma_{\text{ac}} \quad (3)$$

where the values of the dc conductivity (σ_{dc}) are at 100 Hz of the sample.

In the low-frequency region, the curves indicate that our sample exhibits a semiconductor behavior in all temperature range. The experimental curve of dc conductivity is well fitted by the Arrhenius relation [1]:

$$\sigma_{\text{dc}} = \sigma_0 \exp\left(-\frac{E_a}{k_B T}\right) \quad (4)$$

where σ_0 is a pre-exponential factor, E_a is the activation energy for the hopping mechanism, T is the absolute temperature, and k_B is the Boltzmann constant. The plot of $\text{Ln}(\sigma_{\text{dc}})$ versus $(1000/T)$ shown in Fig. 4 for $\text{Ni}_{0.5}\text{Mg}_{0.3}\text{Cu}_{0.2}\text{Fe}_2\text{O}_4$ ferrite nanoparticle is linear in all the 300–500 K temperature range, confirming that conduction process is thermally activated. The E_a value estimated from the slope of the linear fit plot is equal to 0.369 eV. This value is smaller than those of some spinel ferrite systems prepared by different methods for nanoparticles [1, 27–30], which suggest that the conduction mechanism in the sample of the present investigation may be due to hopping of electrons between Fe^{2+} and Fe^{3+} rather than polarons. On the other hand, the value of activation energy obtained for $\text{Ni}_{0.5}\text{Mg}_{0.3}\text{Cu}_{0.2}\text{Fe}_2\text{O}_4$ ferrite sample is lower than those obtained for the $\text{Ni}_{0.5}\text{Mg}_{0.5}\text{Fe}_2\text{O}_4$ ferrite nanoparticle in Refs. [14, 17]. Then, we can conclude that the substitution of 20% of Cu in $\text{Ni}_{0.5}\text{Mg}_{0.5}\text{Fe}_2\text{O}_4$ ferrite system can improve its conductivity.

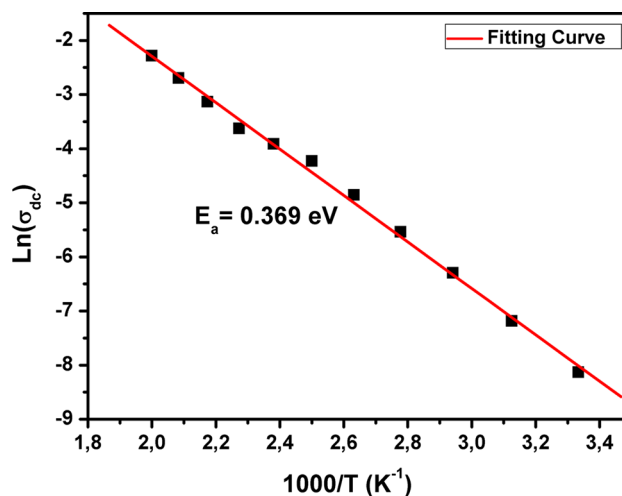


Fig. 4 Variation of the $\text{Ln}(\sigma_{\text{dc}})$ as a function of $(1000/T)$ for $\text{Ni}_{0.5}\text{Mg}_{0.3}\text{Cu}_{0.2}\text{Fe}_2\text{O}_4$ ferrite nanoparticle sintered at 1473 K. Red solid line is the linear fit for data using the Arrhenius relation

For high-frequency region, the ac conductivity (σ_{ac}) can be described by the following power law:

$$\sigma_{ac} = A\omega^n, \quad (5)$$

where A is coefficient-dependent on temperature and n is the frequency exponent which depends on both frequency and temperature. According to Funke [31], the value of n has a physical meaning. $n \leq 1$ means that the electron hopping involves a translational motion with a sudden hopping, whereas $n > 1$ means that the motion involves localized hopping between neighboring sites. The exponent n is frequency-independent, but it depends on both temperature and material kind.

The experimental data of total conductivity shown in Fig. 3 for Ni_{0.5}Mg_{0.3}Cu_{0.2}Fe₂O₄ ferrite nanoparticle were well fitted using Eq. (3). Figure 5 depicts a typical example of this fitting at $T = 300$ K. In the fitting procedure, the (A) and (n) factors have been varied simultaneously to get the best fit. It can be seen that the fit matches well with the experimental values (red solid lines in Fig. 5). The goodness of the fit is usually evaluated by comparing the squared coefficient of linear correlation coefficient (R^2) obtained for each temperature (see Table 1). It is clear from Table 1 (see also the inset of Fig. 5) that n increases with increasing temperature. The change in n with temperature corresponds to a thermally activated process. The temperature dependence of n gives information to specify the suitable mechanism involved for ac conductivity. In our case, the n exponent is superior than 1 for all temperatures, indicating that the electron hopping between Fe²⁺ and Fe³⁺ occurs between neighboring sites.

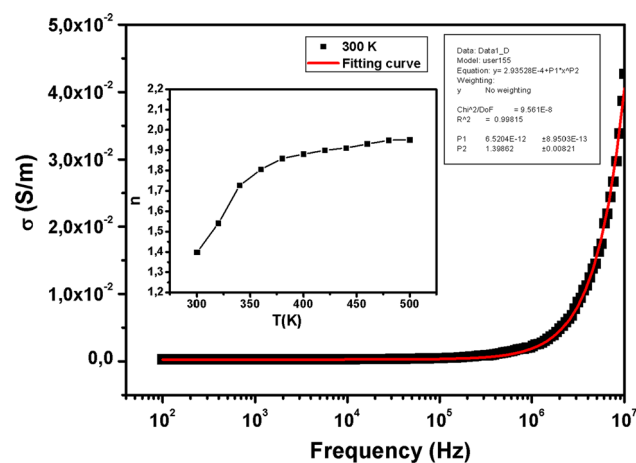


Fig. 5 Variation of the total conductivity versus frequency at $T = 300$ K for Ni_{0.5}Mg_{0.3}Cu_{0.2}Fe₂O₄ ferrite nanoparticle sintered at 1473 K. Red solid lines represent the fitting to the experimental data using the universal Jonscher power law. The inset shows the variation of exponent n with respect to all temperatures

Table 1 Fitting parameters obtained from experimental data of the total conductivity as a function of frequency and temperature using Jonscher power law: $\sigma(\omega) = \sigma_{dc} + A\omega^n$

T (K)	σ_{dc} (S/m) $\times 10^{-3}$	$A \times 10^{-13}$	n	R^2
300	0.294	65.204	1.398	0.998
320	0.757	11.061	1.541	0.998
340	1.84	1.314	1.727	0.999
360	3.94	1.108	1.805	0.997
380	7.79	0.651	1.860	0.997
400	14.54	0.886	1.881	0.999
420	19.96	0.649	1.90	0.999
440	26.61	0.4817	1.911	0.999
460	43.5	0.435	1.931	0.999
480	67.59	0.343	1.949	0.999
500	101.91	0.291	1.952	0.996

3.3 Complex impedance analysis

Figure 6 and its inset show the variation of the real part of impedance (Z') with frequency at various temperatures for Ni_{0.5}Mg_{0.3}Cu_{0.2}Fe₂O₄ ferrite nanoparticle sintered at 1473 K. Figure 6 shows that the magnitude of Z' is typically higher in the low-frequency region and then it decreases gradually with increasing frequency. The value of Z' appears to merge in the high-frequency region irrespective of temperature. This result may possibly be related to the release of space charge as a result of reduction in the barrier properties of material with rise in temperature, and may be a responsible factor for the enhancement of conductivity of the material with temperature at high

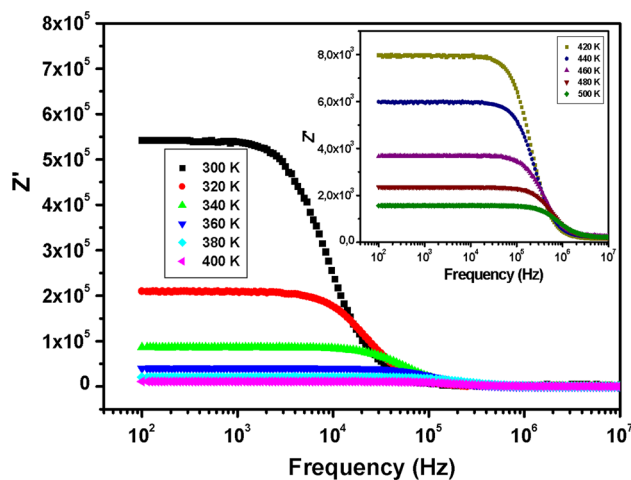


Fig. 6 Main panel: variation of real part of the impedance (Z') as a function of frequency in the temperature range 300–400 K for Ni_{0.5}Mg_{0.3}Cu_{0.2}Fe₂O₄ ferrite nanoparticle sintered at 1473 K. The inset shows the variation of Z' versus f in the temperature range 420–500 K

frequencies. The merging of the value of Z' for all temperatures at higher frequencies can be interpreted by the presence of space charge polarization. This interpretation was confirmed by the higher impedance values at lower frequencies. The behavior of Z' observed for our sample at lower and higher frequencies is in good agreement with the reported results in the literature for several ferrite systems [8, 32, 33].

The variation of Z'' with frequency at different temperatures is depicted in Fig. 7. The spectra of Z'' are characterized by the appearance of peaks which shift to higher frequencies with increasing temperature. Such behavior indicates the existence of relaxation phenomenon in our material. The position of these peaks allows the determination of the relaxation frequency value (f_{max}) and the relaxation time (τ) using the following relation:

$$\tau = 1/2\pi f_{max} \tag{6}$$

Figure 8 shows the plot of $\text{Ln}(\tau)$ versus $1000/T$. We observed that the value of τ decreases with the rise in temperature, which suggests the thermally activated process. The temperature-dependent characteristics of τ follow the Arrhenius relation as mentioned below [1]:

$$\tau = \tau_o \exp\left(\frac{E_a}{k_B T}\right) \tag{7}$$

where E_a is the activation energy. The E_a value estimated from the slope of the linear fit plot (see Fig. 8) is equal to 0.351 eV. This value is in good agreement with those previously derived from the analysis of the dc conductivity. The small difference (0.018 eV) in the activation energy for the conduction and relaxation may be due to the fact that the relaxation process involves only the hopping

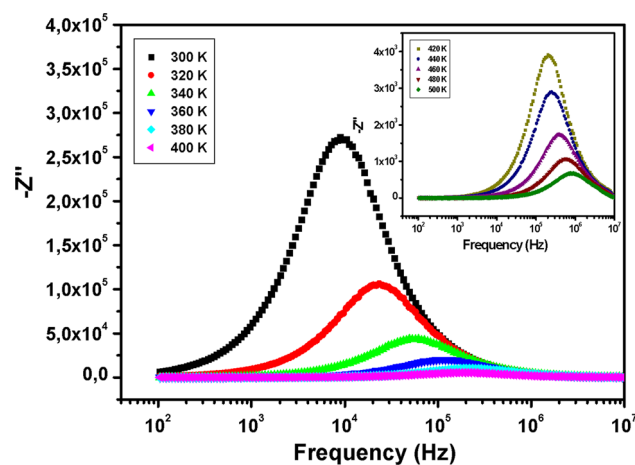


Fig. 7 Main panel: variation of imaginary part of the impedance (Z'') as a function of frequency in the temperature range 300–400 K for $\text{Ni}_{0.5}\text{Mg}_{0.3}\text{Cu}_{0.2}\text{Fe}_2\text{O}_4$ ferrite nanoparticle sintered at 1473 K. The inset shows the variation of Z' versus f in the temperature range 420–500 K

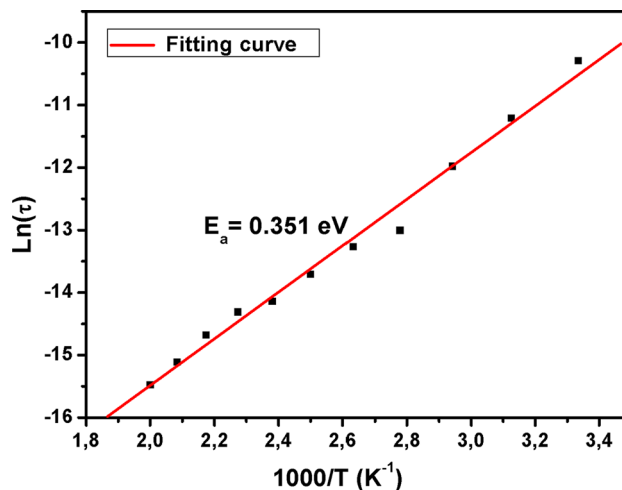


Fig. 8 Variation of the $\text{Ln}(\tau)$ as a function of $(1000/T)$ for $\text{Ni}_{0.5}\text{Mg}_{0.3}\text{Cu}_{0.2}\text{Fe}_2\text{O}_4$ ferrite nanoparticle sintered at 1473 K. Red solid line is the linear fit for our data

energy of the carriers between the localized states, but the conduction mechanism involves hopping energy as well as disorder and binding energy of polarons [34]. From this, we can conclude that the same type of charge carrier is responsible for the conduction and relaxation process. This is in good agreement with the results found in Ref. [1].

If we plot the $Z''(f, T)$ data in the scaled coordinates, i.e., $Z''(f, T)/Z''_{max}$ and $\log(f/f_{max})$, where f_{max} corresponds to the frequency of the peak value of Z'' in the Z'' versus $\log(f)$ plots, the entire data of imaginary part of impedance can collapse into one master curve as shown in Fig. 9. Thus, the scaling behavior of Z'' clearly indicates that the relaxation mechanism is nearly temperature-independent [1, 35, 36].

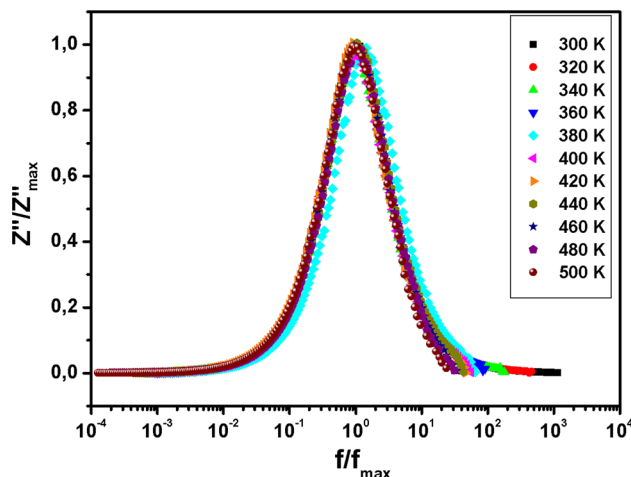


Fig. 9 Scaling behavior of Z'' at various temperatures for $\text{Ni}_{0.5}\text{Mg}_{0.3}\text{Cu}_{0.2}\text{Fe}_2\text{O}_4$ ferrite nanoparticle sintered at 1473 K

The complex-plane impedance plots (called Nyquist plots, i.e., Z'' vs. Z' plot) for different temperatures for Ni_{0.5}Mg_{0.3}Cu_{0.2}Fe₂O₄ ferrite nanoparticle sintered at 1473 K are illustrated in Fig. 10. One of the important factors, which influence the impedance properties of ferrites, is the microstructural effect [19]. The impedance measurement gives us information about the resistive (real part) and reactive (imaginary part) components of a material. A ferrite material is assumed to be consisting of piled-up crystalline plates. From the microstructural point of view, a sample is assumed as a microstructure made up of parallel conducting plates (grains) separated by resistive plates (grain boundaries). For all temperatures, as evident in Fig. 10, the impedance spectra show semicircle arcs (whose maxima and diameters decrease with increasing temperature) that are due to the conduction of the grain boundary, suggesting that a predominant conduction is through the grain boundary volume. Furthermore, contribution from the grain is not well resolved for all temperatures. It is therefore concluded that the conductivity for our sample is mainly due to the grain boundary contribution [19, 37]. To confirm this, it is necessary to modelize the sample. The appropriate equivalent circuit configuration for the impedance plane plots is of the type of $(R_g + R_{gb}/C_{gb})$ [38, 39], as shown in the inset of Fig. 10. R_g and R_{gb} modelize the grain and grain boundary resistances, respectively, and the capacitance (C_{gb}) modelizes the grain boundary capacitance. The intersection with real axis of the semicircle at low frequencies (right intersect) is ascribed to the total resistance ($R_T = R_g + R_{gb}$). On the other hand, the impedance response of grain dominates at high frequencies, so R_g can be deduced from the left

intersect of the semicircle with real axis. The grain boundary resistance values are then given as $R_{gb} = R_T - R_g$. From the impedance spectra represented in Fig. 10, it is clear that the grain resistance R_g is too weak and the grain boundary is approximately equal to R_T . The expression of real (Z') and imaginary (Z'') components of impedance related to the equivalent circuit is [40]:

$$Z' = R_g + \frac{R_{gb}}{1 + R_{gb}^2 C_{gb}^2 \omega^2} \tag{8}$$

$$Z'' = \frac{R_{gb}^2 C_{gb} \omega}{1 + R_{gb}^2 C_{gb}^2 \omega^2} \tag{9}$$

The impedance data for all temperatures are fitted using Zview software [41]. It can be seen that the fit matches well with the experimental values (red solid lines in Fig. 10). The values of all fitted parameters are presented in Table 2. It can be seen from this table that the grain boundary resistance decreases with the increase in temperature, indicating a semiconducting behavior of our sample. The decrease in grain boundary resistance is due to the fact that the grain boundary effect has assisted in lowering the barrier to the motion of charge carriers paving the way for increased electrical transport with rise in temperature. Furthermore, it has been found that the values of R_{gb} are larger than R_g which indicates that the conductivity for our sample is mainly due to the grain boundary contribution as mentioned above.

3.4 Dielectric properties

Figure 11a shows the frequency dependence of the imaginary part of dielectric constant (ϵ'') at different temperatures for Ni_{0.5}Mg_{0.3}Cu_{0.2}Fe₂O₄ ferrite nanoparticle sintered

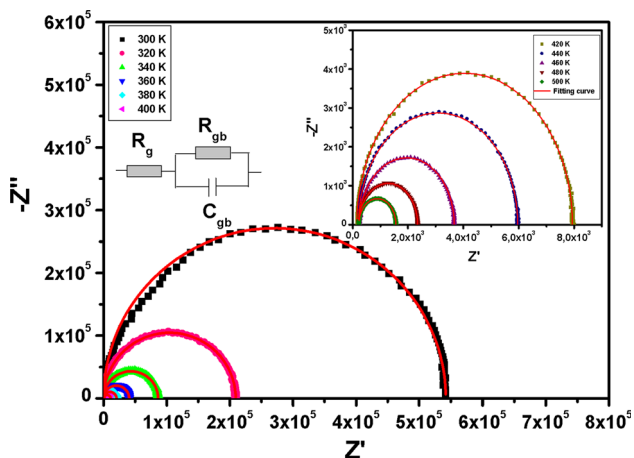


Fig. 10 Main panel: Nyquist plots (Z'' vs. Z') in the temperature range 300–400 K for Ni_{0.5}Mg_{0.3}Cu_{0.2}Fe₂O₄ ferrite nanoparticle sintered at 1473 K. The inset shows the Nyquist plots in the temperature range 420–500 K. Red solid lines represent the fitting to the experimental data according to the appropriate equivalent circuit (see the inset)

Table 2 Electrical parameters of equivalent circuit deduced from complex impedance spectrum for different temperatures for Ni_{0.5}Mg_{0.3}Cu_{0.2}Fe₂O₄ ferrite nanoparticle

T (K)	R_g (Ω)	R_{gb} (Ω)	$C_{gb} \times 10^{-11}$ (F)
300	233	542,290	3.232
320	230	209,310	3.263
340	222	86,318	3.253
360	189	4037	3.400
380	149	20,234	3.543
400	105	10,651	8.133
420	75	7788	9.845
440	65	5749	10.84
460	40	3440	11.73
480	31	2124	13.02
500	20	1339	14.17

T temperature, R_g grain resistance, R_{gb} grain boundary resistance, C_{gb} grain boundary capacitance

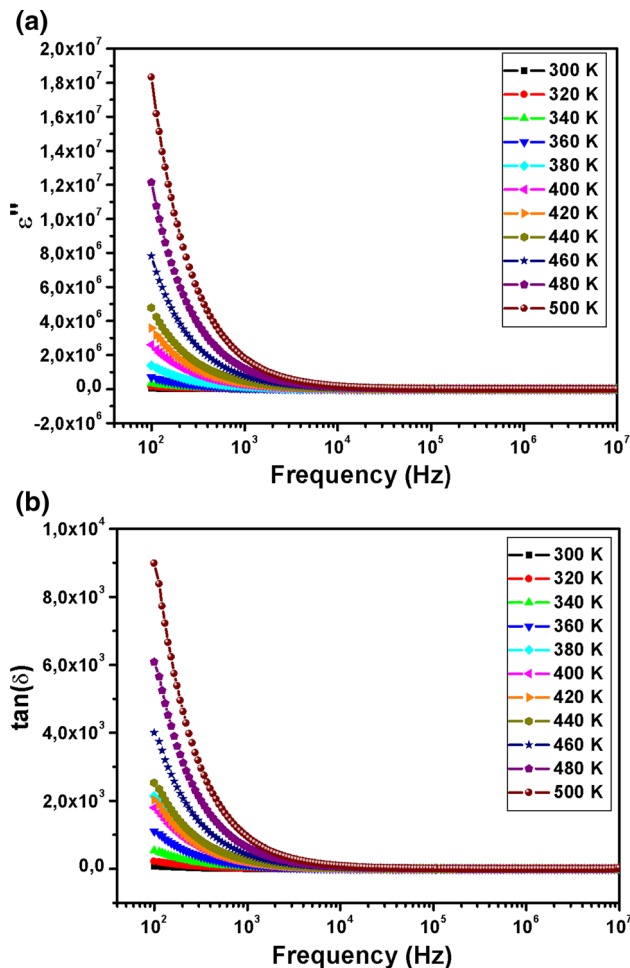


Fig. 11 Frequency dependence at different temperatures of **a** imaginary part of dielectric constant (ϵ'') and **b** dielectric loss factor ($\tan\delta$) of $\text{Ni}_{0.5}\text{Mg}_{0.3}\text{Cu}_{0.2}\text{Fe}_2\text{O}_4$ ferrite nanoparticle sintered at 1473 K

at 1473 K. The values of ϵ'' were calculated from the conductivity data using the following relation:

$$\epsilon'' = \frac{\sigma}{\omega\epsilon_0} \quad (10)$$

where $\omega = 2\pi f$ is the angular frequency and $\epsilon_0 = 8.854 \times 10^{-12}$ F/m is the permittivity of free space. It is observed from Fig. 11a that ϵ'' values decrease with increase in frequency. This type of dielectric behavior in the ferrite has been explained by the Maxwell–Wagner and Koop’s phenomenological theory [42]. Accordingly, the dielectric structure of ferrites is made up of well-conducting layer of grains followed by poorly conducting layer of grain boundaries, and the high value of dielectric constant arises from the space charge polarization produced at the grain boundary. The polarization mechanism involves the exchange of electrons between the ions of the same element, which are present in more than one valence states and are distributed randomly over crystallographic

equivalent sites. Here the exchange of electrons mainly takes place between Fe^{3+} and Fe^{2+} ions present at octahedral sites (B-site). During this exchange mechanism, the electrons have to pass through the grains and grain boundary of the dielectric medium. Owing to high resistance of the grain boundary, the electrons accumulate at the grain boundary and produce space charge polarization. Figure 11a also shows that the dielectric constant (ϵ'') decreases rapidly in the low-frequency region and becomes frequency-independent in the high-frequency region. It is well known that the grain boundaries are more effective in low-frequency region and the grains are effective in the high-frequency region [42]. Therefore, due to the grain boundary effect, the dielectric constant decreases rapidly in the low-frequency region. In the high-frequency region, the grains come into action and also the hopping of electrons cannot follow the high-frequency *ac* field; therefore, the dielectric constant decreases and becomes frequency-independent. It is also observed from Fig. 11a that ϵ'' increases with increase in temperature because the hopping of charge carriers at the octahedral site is thermally activated.

The dielectric loss factor ($\tan\delta$) was calculated using the following relation:

$$\tan(\delta) = \frac{Z'}{Z''} \quad (11)$$

This factor is a measure of dielectric loss within the ferrite, and it arises when the polarization lags behind the applied *ac* field. The variation of $\tan\delta$ with frequency at different temperatures for $\text{Ni}_{0.5}\text{Mg}_{0.3}\text{Cu}_{0.2}\text{Fe}_2\text{O}_4$ ferrite nanoparticle is shown in Fig. 11b. The dielectric loss $\tan\delta$ decreases rapidly in the low-frequency region, and in the high-frequency region, it becomes almost frequency-independent. Such a behavior can be explained on the basis that in the low-frequency region, which corresponds to low conductivity of grain boundary, more energy is required for electron exchange between Fe^{2+} and Fe^{3+} ions; as a result, the loss is higher. In the high-frequency region, which corresponds to high conductivity of grain, a small energy is required for electron transfer between the $\text{Fe}^{2+}/\text{Fe}^{3+}$ ions at the octahedral site. Further, the loss increases with increasing temperature due to the increased conduction of thermally activated electrons (Fig. 11b).

4 Conclusion

$\text{Ni}_{0.5}\text{Mg}_{0.3}\text{Cu}_{0.2}\text{Fe}_2\text{O}_4$ ferrite nanoparticle has been prepared by sol–gel technique. The XRD patterns reveal the spinel structure of the sintered ferrite. Conductivity is constant in the low-frequency region and shows dispersion in the high-frequency region. The linear variation of

conductivity with temperature confirms the semiconducting nature of the studied sample. The curves of imaginary part of impedance (Z'') show the presence of electrical relaxation phenomenon in our sample with an activation energy close to that determined from dc conductance curve. The Nyquist representations (Z'' vs. Z') revealed the appearance of semicircle arcs, well modelled in terms of electrical equivalent circuit of the type of ($R_g + R_{gb}/C_{gb}$). Dielectric constant (ϵ'') and dielectric loss ($\tan\delta$) decrease with the frequency of external electric field and increase with the increase in temperature. This has been explained in terms of hopping of charge carriers between Fe²⁺ and Fe³⁺ ions.

References

- S.K. Mandal, S. Singh, P. Dey, J.N. Roy, P.R. Mandal, T.K. Nath, *J. Alloys Compd.* **656**, 887–896 (2016)
- M. Abdullah Dar, K. Majid, K.M. Batoo, R. Kotnala, *J. Alloys Compd.* **632**, 307–320 (2015)
- V. Jagdeesha Angadi, L. Choudhury, K. Sadhana, H.-S. Liu, R. Sandhya, S. Matteppanavar, B. Rudraswamy, V. Pattar, R.V. Anavekar, K. Praveen, *J. Magn. Magn. Mater.* **424**, 1–11 (2017)
- Z. Liu, Z. Peng, C. Lv, F. Xiuli, *Ceram. Int.* **43**, 1449–1454 (2017)
- R.K. Panda, R. Muduli, G. Jayarao, D. Sanyal, D. Behera, *J. Alloys Compd.* **669**, 19–28 (2016)
- E. Oumezzine, S. Hcini, M. Baazaoui, E.K. Hlil, M. Oumezzine, *Powder Technol.* **278**, 189–195 (2015)
- N. Sivakumar, A. Narayanasamy, K. Shinoda, C.N. Chinmasamy, B. Jeyadevan, J.M. Greneche, *J. Appl. Phys.* **102**, 013916–013923 (2007)
- M. Azizar, A.K.M. Rahman, A. Hossain, *Phys. Scr.* **89**, 025803–025810 (2014)
- B. Ünal, A. Baykal, *J. Supercond. Nov. Magn.* **27**, 469–479 (2014)
- Y. Köseoğlu, *Ceram. Int.* **39**, 4221–4230 (2013)
- Y. Köseoğlu, M. Bay, M. Tan, A. Baykal, H. Sözeri, R. Topkaya, N. Akdoğan, *J. Nanopart. Res.* **13**, 2235–2244 (2011)
- E. Şentürk, Y. Köseoğlu, T. Şaşmaz, F. Alan, M. Tan, *J. Alloys Compd.* **578**, 90–95 (2013)
- M. Hashim, Alimuddin, S. Kumar, S.E. Shirsath, R.K. Kotnala, H. Chung, R. Kumar, *Powder Technol.* **229**, 37–44 (2012)
- M. Naeem, N.A. Shahb, I.H. Gul, A. Maqsood, *J. Alloys Compd.* **487**, 739–743 (2009)
- H. Moradmard, S. Farjami Shayesteh, P. Tohidi, Z. Abbas, M. Khaleghi, *J. Alloys Compd.* **650**, 116–122 (2015)
- L. John Berchmans, R. Kalai Selvan, P.N. Selva Kumar, C.O. Augustin, *J. Magn. Magn. Mater.* **279**, 103–110 (2004)
- M.A. Gabal, Y.M. Al Angari, H.M. Zaki, *J. Magn. Magn. Mater.* **363**, 6–12 (2014)
- M.A. El Hiti, *J. Phys. D Appl. Phys.* **29**, 501–505 (1996)
- M. Hashim, S.S. Meena, R.K. Kotnala, S.E. Shirsath, A.S. Roy, A. Parveen, P. Bhatt, S. Kumar, R.B. Jotania, R. Kumar, Alimuddin, *J. Alloys Compd.* **602**, 150–156 (2014)
- A.K.M.A. Hossain, M.R. Amin, H. Tanaka, *J. Magn. Magn. Mater.* **334**, 124 (2013)
- M.A. El Hiti, *J. Magn. Magn. Mater.* **164**, I87–196 (1996)
- M.S. Anwar, F. Ahmed, B.H. Koo, *Acta Mater.* **71**, 100–107 (2014)
- Y. Köseoğlu, F. Alan, M. Tan, R. Yilgin, M. Öztürk, *Ceram. Int.* **38**, 3625–3634 (2012)
- R.D. Shannon, *Acta Crystallogr. A* **32**, 751–767 (1976)
- J.S. Ghodake, R.C. Kambale, S.V. Salvi, S.R. Sawant, S.S. Suryavanshi, *J. Alloys Compd.* **486**, 830–834 (2009)
- A.K. Jonscher, *Universal Relaxation Law* (Chelsea Dielectrics Press, London, 1996)
- M.S.R. Prasad, K.V. Ramesh, B.R. Babu, K. Trinath, *J. Phys.* **90**, 417–428 (2016)
- A. Humaira, M. Asghari, *J. Phys: Conf. Ser.* **439**, 012014–012020 (2013)
- S. Bhukal, S. Mor, S. Bansal, J. Singh, S. Singhal, *J. Mol. Struct.* **2014**, 95–102 (1071)
- S. Bhukal, T. Namgyal, S. Mor, S. Bansal, S. Singhal, *J. Mol. Struct.* **2012**, 162–167 (1012)
- K. Funke, *Prog. Solid State Chem.* **22**, 111–195 (1993)
- Z. Ahmad, S. Atiq, S.K. Abbas, S.M. Ramay, S. Riaz, S. Naseem, *Ceram. Int.* **42**, 18271–18282 (2016)
- M.-R. Syue, F.-J. Wei, C.-S. Chou, F. Chao-Ming, *Thin Solid Films* **519**, 8303–8306 (2011)
- M. Idrees, M. Nadeem, M.M. Hassan, *J. Phys. D Appl. Phys.* **43**, 155401–155409 (2010)
- V. Mohanty, R. Cheruku, L. Vijayan, G. Govindaraj, *J. Mater. Sci. Technol.* **30**(4), 335–341 (2014)
- A. Sinha, A. Dutta, *RSC Adv* **5**, 100330–100338 (2015)
- K.M. Batoo, *Phys. B* **406**, 382–387 (2011)
- M. Nadeem, M.J. Akhtar, A.Y. Khan, R. Shaheen, M.N. Hoqu, *Chem. Phys. Lett.* **366**, 433 (2002)
- M. Nadeem, M.J. Akhtar, A.Y. Khan, *Solid State Commun.* **134**, 431 (2005)
- H. Rahmouni, M. Nouiri, R. Jemai, N. Kallel, F. Rzigua, A. Selmi, K. Khirouni, S. Alaya, *J. Magn. Magn. Mater.* **316**, 23–28 (2007)
- D. Johnson, *ZView: a Software Program for IES Analysis, Version 2.8*, Scribner Associates, Inc. Southern Pines, NC (2008)
- C.G. Koops, *Phys. Rev.* **83**, 121–124 (1951)